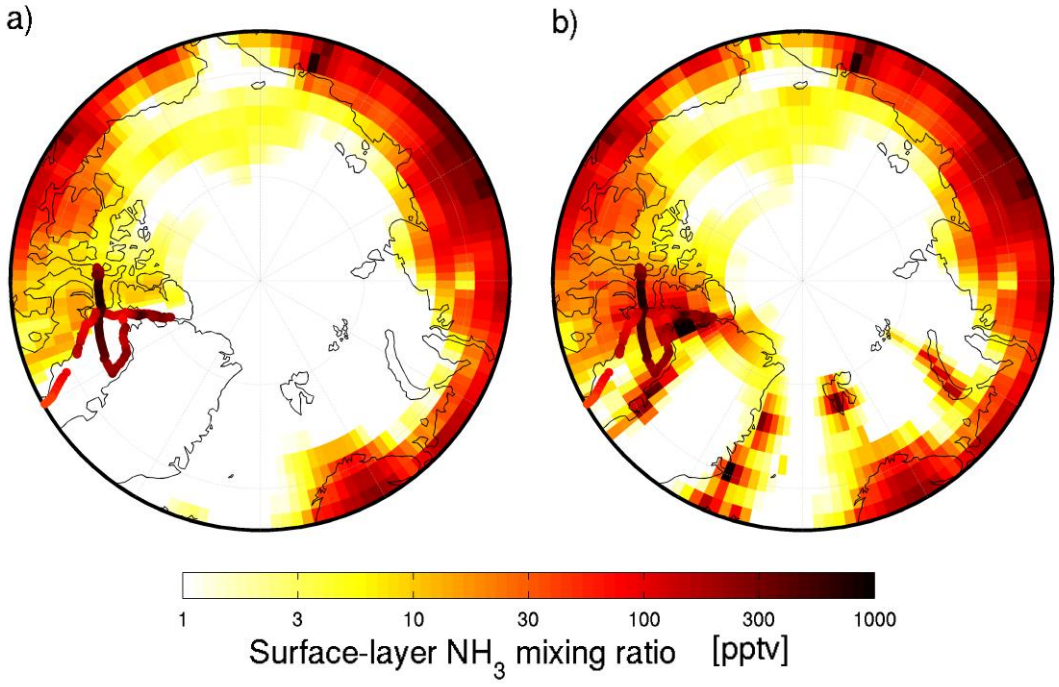

Supplementary Fig. 1: Simulated and observed Arctic surface-layer ammonia. Geographic distribution of GEOS-Chem-TOMAS-simulated July-August mean surface-layer ammonia (NH_3) mixing ratios a) without the seabird-colony NH_3 emissions inventory and b) with the seabird-colony NH_3 emissions inventory implemented. The NH_3 mixing ratios measured along the July-August 2014 NETCARE ship track are superimposed as circles in the Baffin Bay, Lancaster Sound and Nares Strait regions.

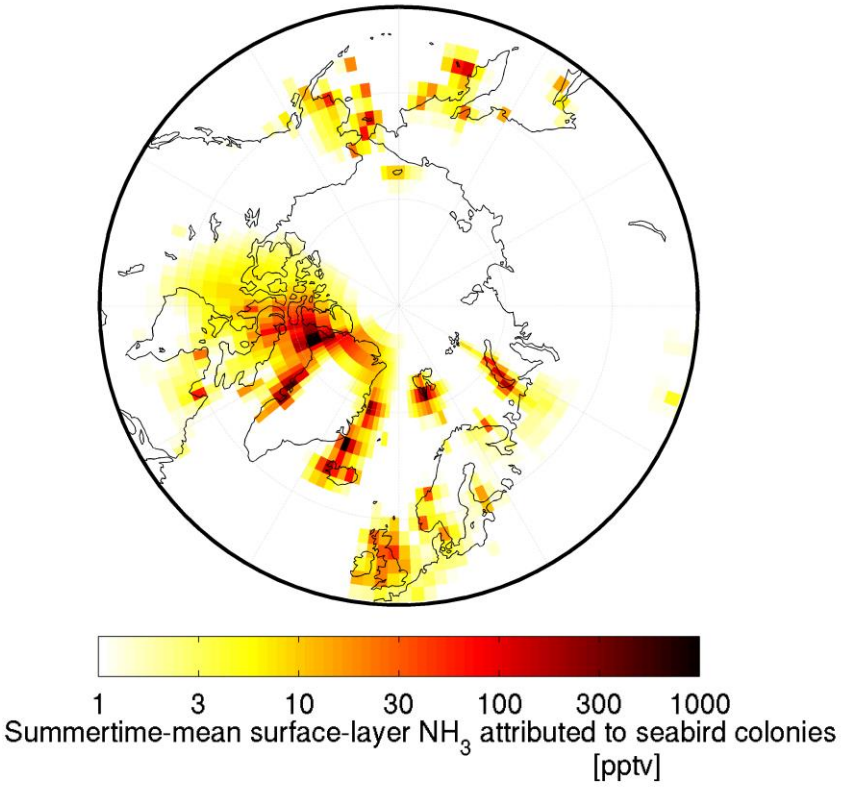

Supplementary Fig. 2: Simulated Arctic surface-layer NH_3 attributed to seabird-colony emissions.

Geographic distribution of GEOS-Chem-TOMAS-simulated July-August mean surface-layer ammonia (NH_3) mixing ratio attributed to seabird-colony NH_3 emissions based on simulations with versus without the seabird-colony NH_3 emissions.

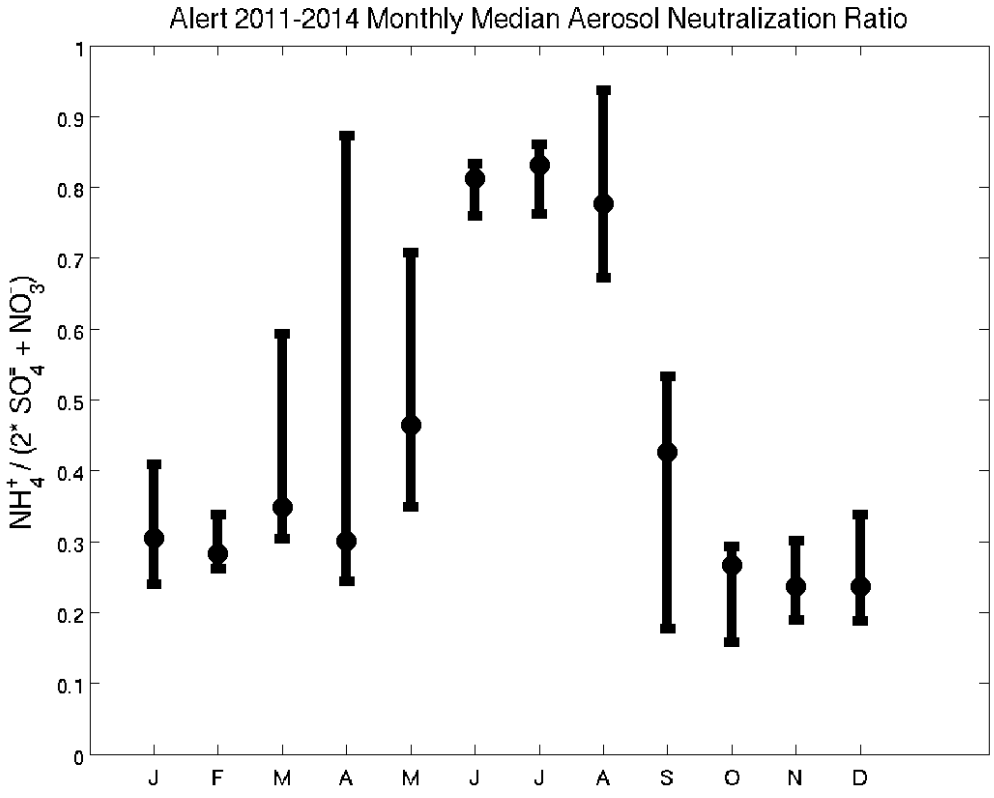

Supplementary Fig. 3: Alert measurement neutralization ratio.

Monthly median neutralization ratio from ion chromatography analysis of weekly filter samples from March 2011 to December 2014 at Alert. The error bars indicate the 25th and 75th percentiles.

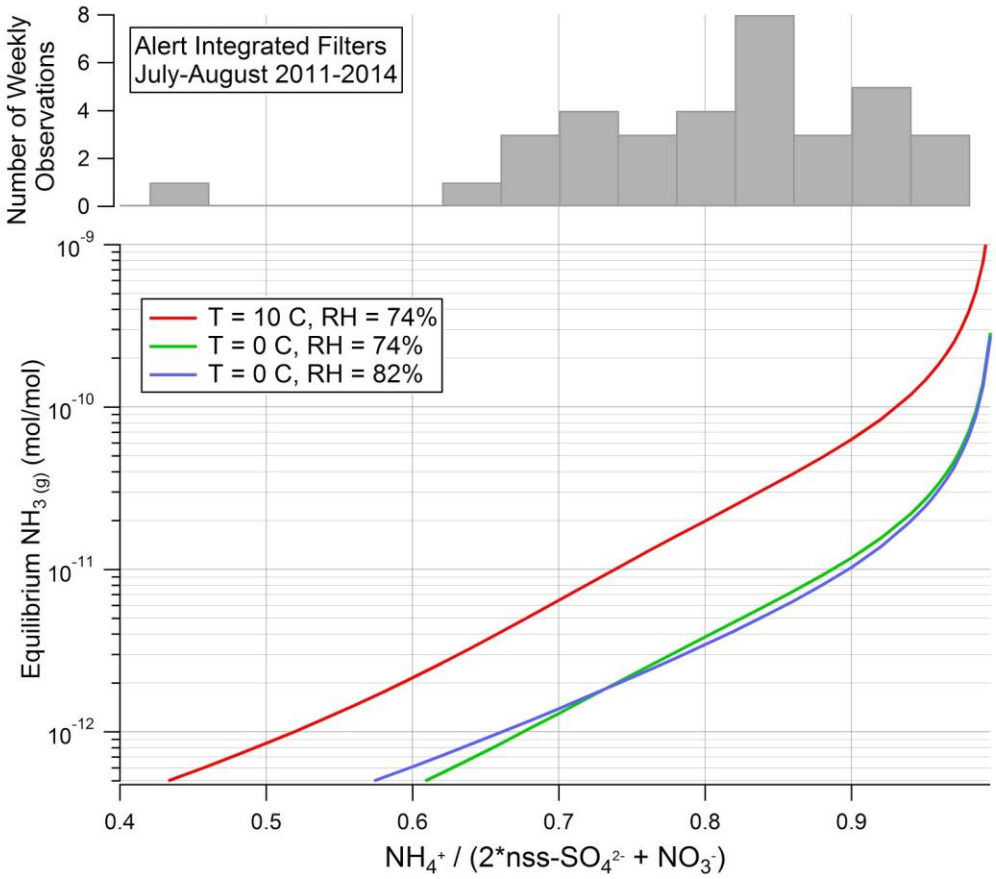

Supplementary Fig. 4: Alert measurement neutralization ratio frequency and NH_3 equilibrium calculations.

Top panel: Frequency of observing different ratios of $NH_4^+/(2nss\text{-}SO_4^{2-} + NO_3^-)$ on weekly integrated filters collected at Alert during the months of July and August 2011-2014 and analyzed by ion chromatography. Bottom panel: Mixing ratio of gas phase NH_3 calculated to be in equilibrium with different ratios of $NH_4^+/(2nss\text{-}SO_4^{2-} + NO_3^-)$, depending on the temperature and relative humidity. Calculations were performed using the Extended Aerosol Inorganics Model (E-AIM) Model II[1,2]. The model is accessible online at (http://www.aim.env.uea.ac.uk/aim/model2/model2a.php). The solute inputs to the modelled systems were restricted to $nssSO_4^{2-}$ (non-sea salt sulphate), NO_3^-, H^+, and NH_4^+, and the formation of solids was turned off to model deliquesced aerosol.

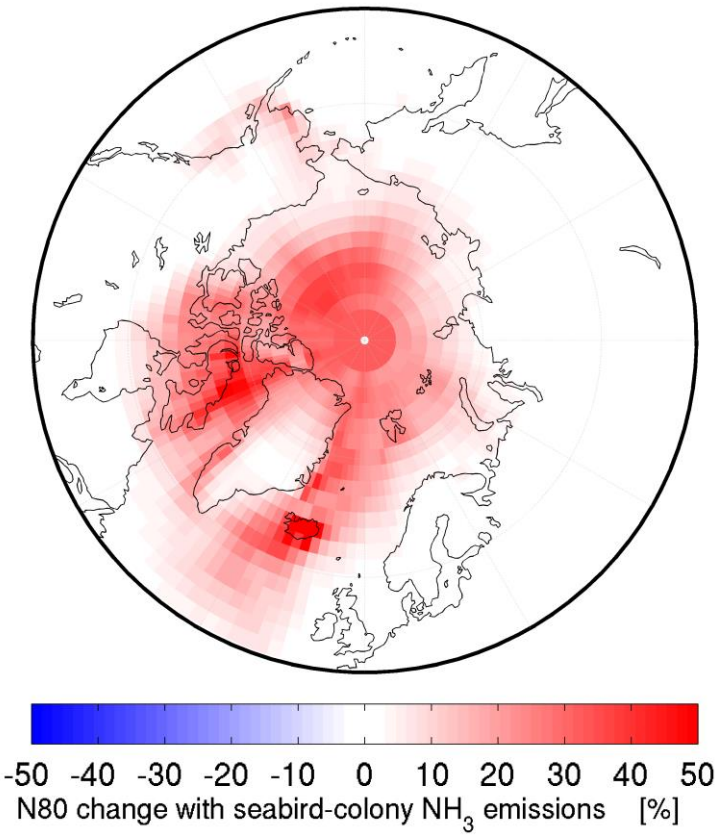

Supplementary Fig. 5: Change in simulated particle number concentrations.

Geographic distribution of the percent change in summertime-mean number concentration of particles with diameters larger than 80 nm (N80) for the GEOS-Chem-TOMAS simulations with versus without seabird-colony NH_3 emissions implemented.

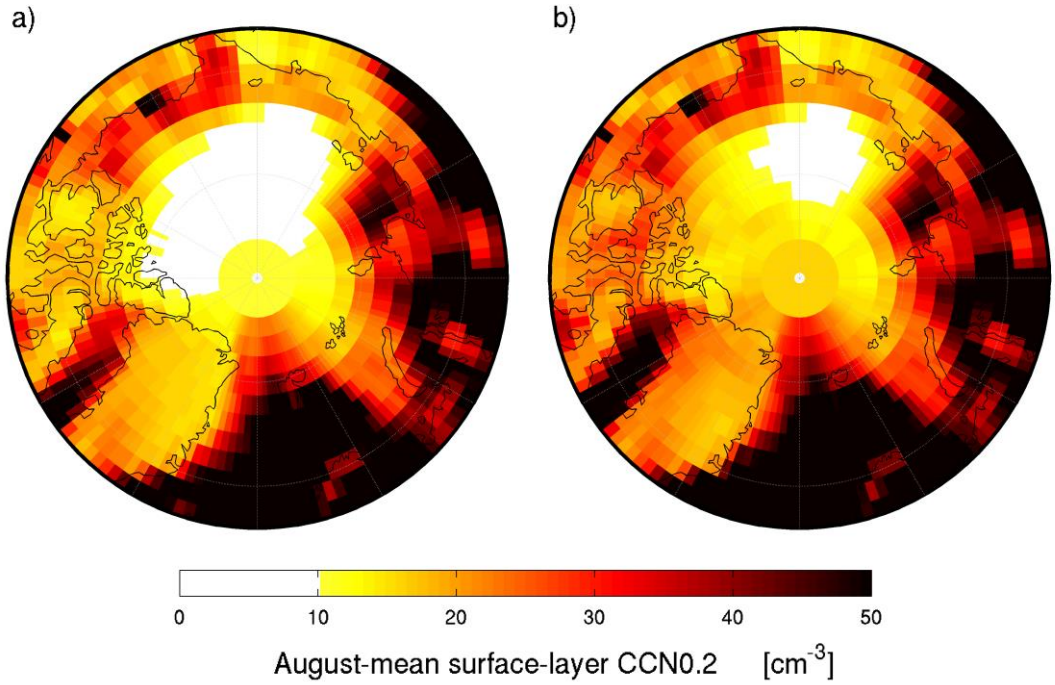

Supplementary Fig. 6: Simulated cloud-condensation nuclei concentrations.

Simulated August-mean surface-layer cloud-condensation nuclei concentration at 0.2% supersaturation (CCN0.2) for the simulation a) without seabird-colony NH_3 emissions and b) with seabird-colony NH_3 emissions.

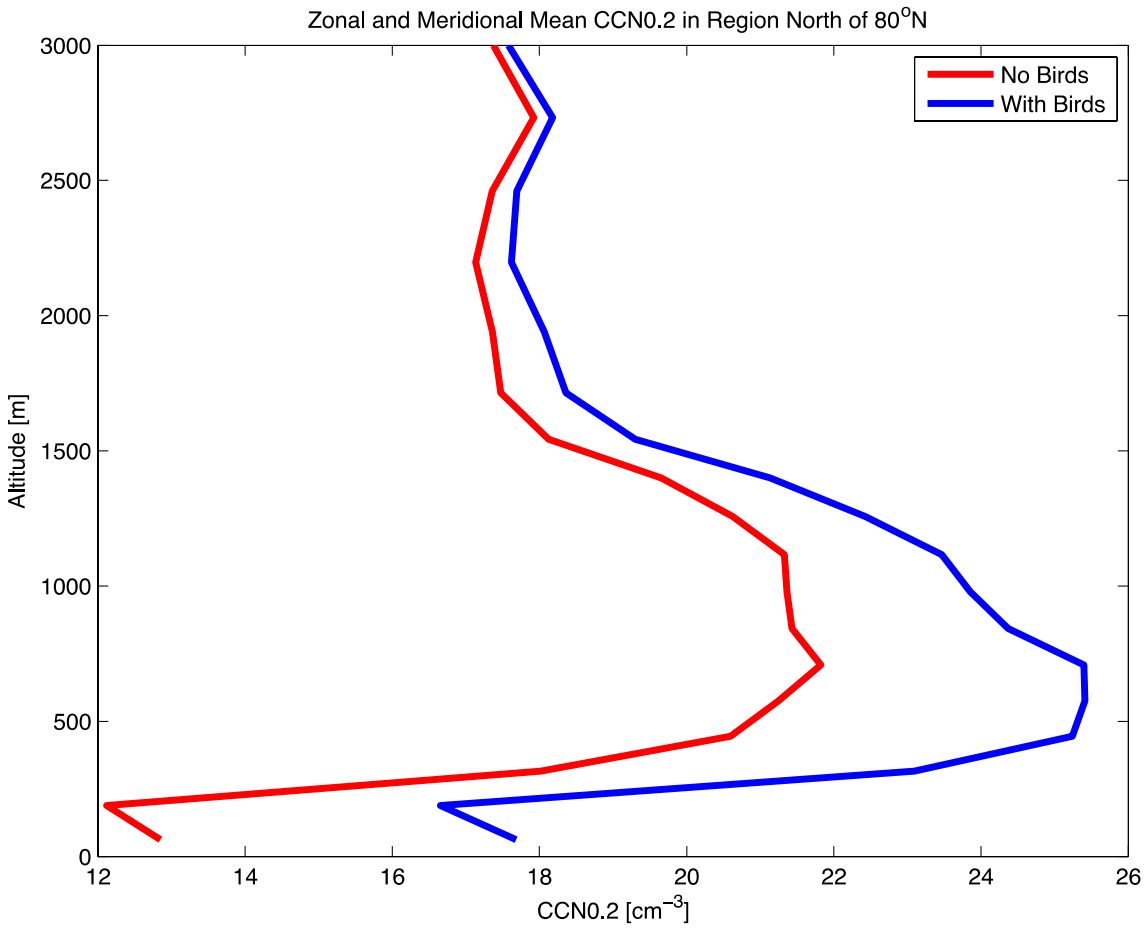

Supplementary Fig. 7: High Arctic mean simulated cloud-condensation nuclei concentrations.

August zonal and meridional mean vertical profile of cloud condensation nuclei at 0.2% supersaturation (CCN0.2) for the region north of 80 °N including all longitudes for the simulations without (red) and with (blue) seabird-colony ammonia emissions, respectively.

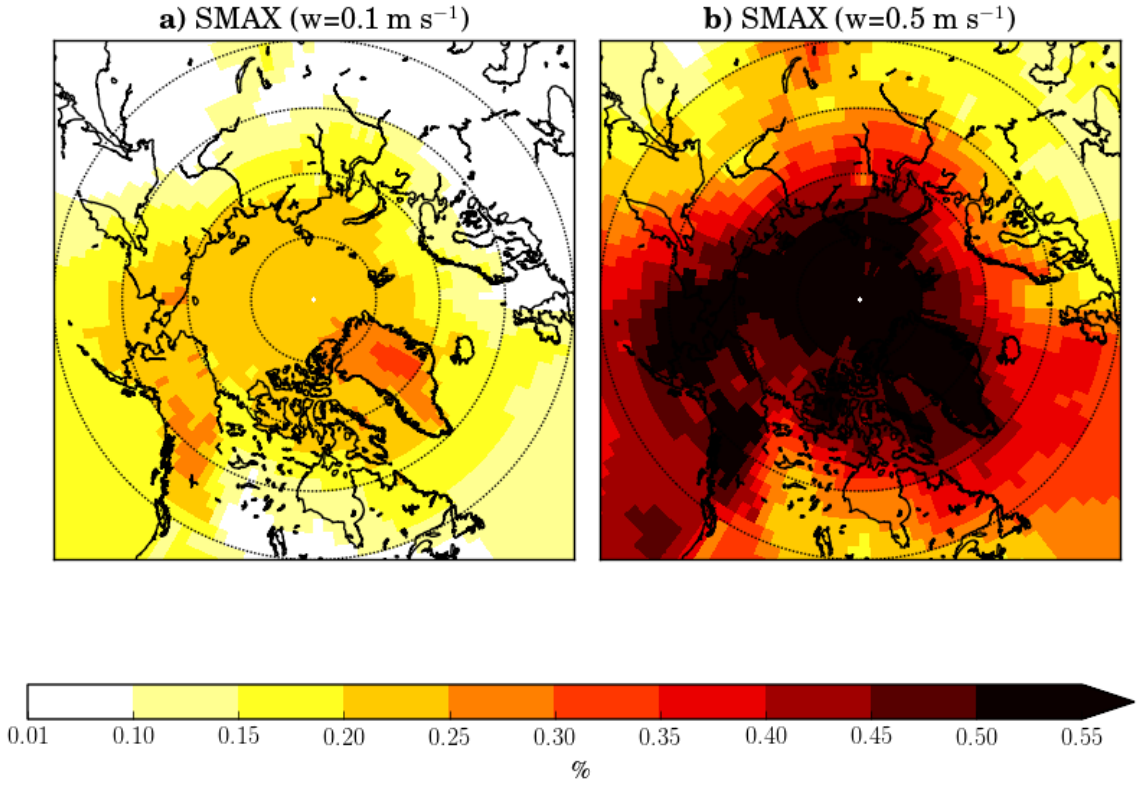

Supplementary Fig. 8: Simulated supersaturation.

Summertime-mean maximum supersaturation calculated assuming a constant updraft of a) 0.1 m s^{-1} and b) 0.5 m s^{-1}.

.

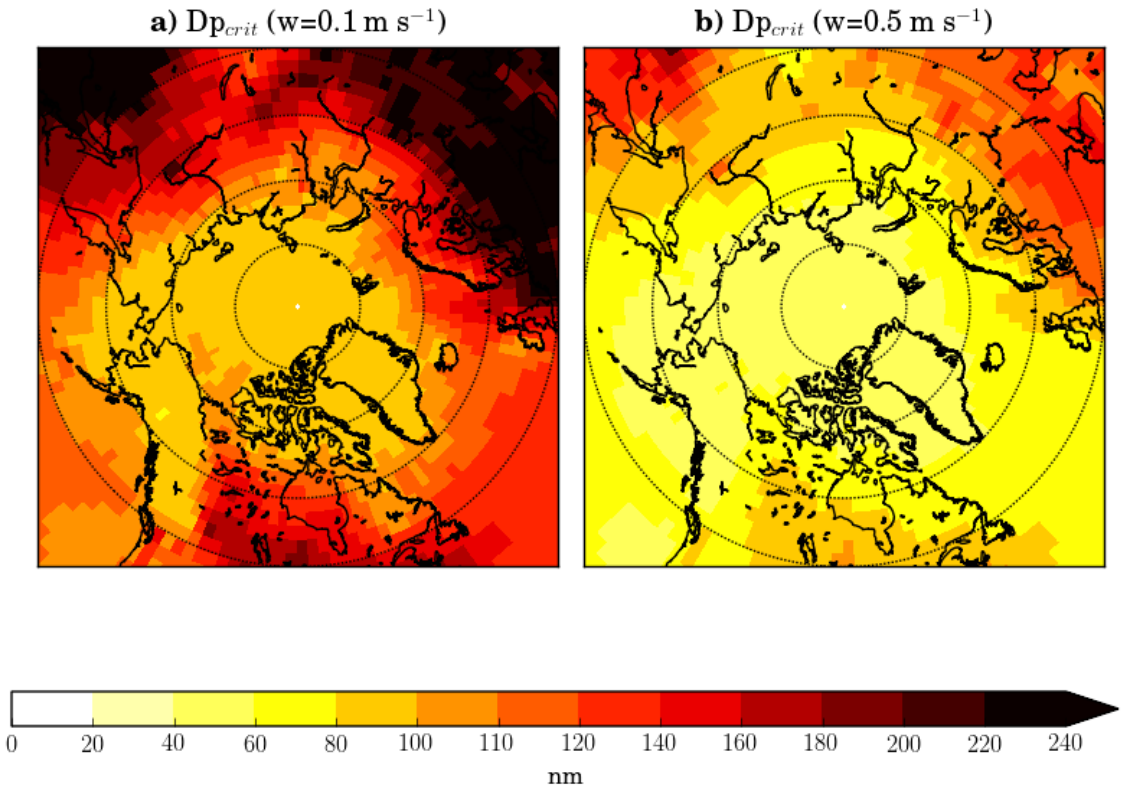

Supplementary Fig. 9: Simulated particle activation diameter.

Minimum particle diameter activating to form cloud droplets in our summertime simulations with updraft speeds of a) 0.1 m s^{-1} and b) 0.5 m s^{-1}.

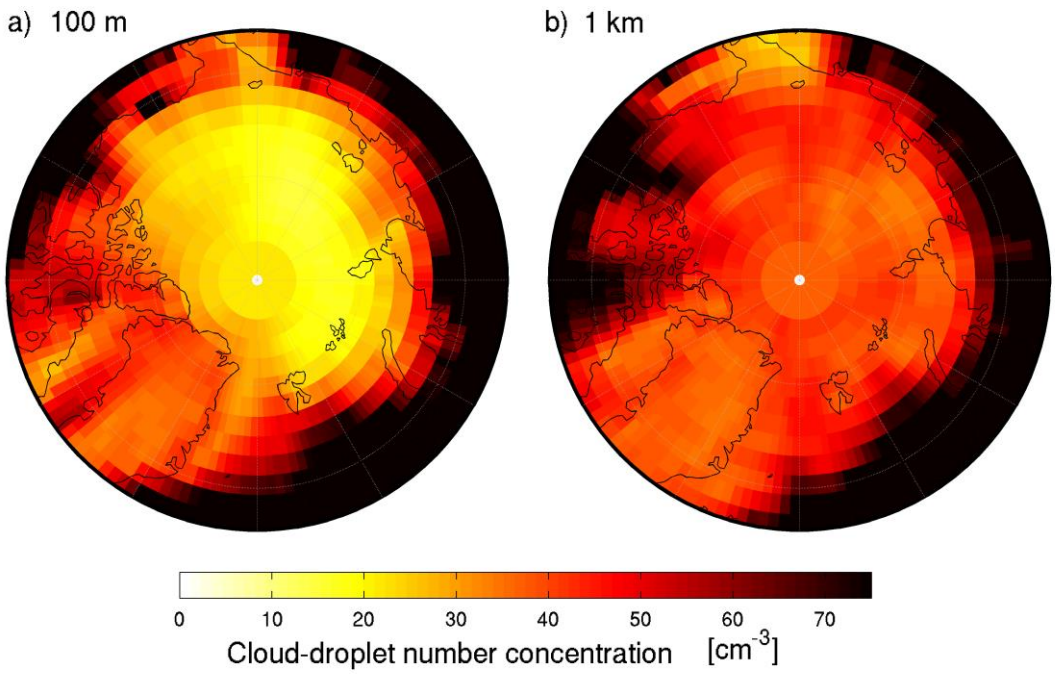

Supplementary Fig. 10: Simulated cloud-droplet number concentration.

Simulated summertime-mean pan-Arctic cloud-droplet number concentration (CDNC) [cm^{-3}] at about a) 100 m and b) 1 km for the GEOS-Chem-TOMAS simulation with the seabird-colony emissions and with assumed 0.5 m s^{-1} updraft speed.

Supplementary Table 1: Instrument detection limits. Detection limits for methyl- and ethyl- amines for the AIM-IC instrument.

Amine	Gas-phase (pptv)	Particulate-phase (ng m^{-3})
Monomethylamine (MMA)	0.43	0.6
Dimethylamine (DMA)	0.48	0.97
Monoethylamine (MEA)	0.44	0.88
Diethylamine (DEA) and Trimethylamine (TMA)*	0.49	1.45
Triethylamine (TEA)	0.46	2.07

*These species co-elute and could not be distinguished.

Supplementary Table 2: Sensitivity studies. Pan-Arctic mean aerosol indirect effect (AIE) in W m^{-2} over the oceans attributed to seabird-colony ammonia for the standard simulation and set of sensitivity studies as described in Methods.

Simulation Name	AIE (W m^{-2})
Standard	-0.46
2xNH3	-0.62
0.5xNH3	-0.26
simMSA	-0.84
simPOA	-0.36
simvel0.1	-0.38
simvel1.0	-0.54

Supplementary Table 3: Seabird-colony ammonia (NH_3) emissions. NH_3 emissions implemented in addition to the Riddick et al.[3,4] seabird-colony NH_3 inventory at latitudes between 50 °N and 60 °N.

Latitude (°N)	Longitude (°E)	Emissions (Mg NH_3 yr^{-1})
51.2	156.6	58.2
55.1	-132.8	19.5
55.8	-156.1	436.5
56.9	-169.9	853.7
57.0	-158.7	550.6
57.1	-135.5	13.9
57.2	-153.8	97.4
59.0	-161.9	811.2
59.0	-154.4	5.2
59.0	-137.9	2.7
59.1	149.1	109.7
59.7	-150.3	131.2

Supplementary Table 4: Seabird-colony ammonia (NH_3) emissions. NH_3 emissions implemented in addition to the Riddick et al.[3,4] seabird-colony NH_3 inventory at latitudes between 60 °N and 70 °N.

Latitude (°N)	Longitude (°E)	Emissions (Mg NH_3 yr^{-1})
60.0	-144.9	187.6
60.0	-141.2	0.9
60.2	-164.8	66.5
60.4	-172.7	366.6
60.7	-146.6	68.8
64.1	-172.3	663.4
64.3	-161.5	89.0
64.7	-166.4	30.4
65.0	37.3	18.3
65.4	-176.5	12.1
65.5	34.0	2.6
66.4	36.6	2.0
67.1	-163.9	102.6
68.2	29.9	5.5
68.6	-166.1	110.6
69.3	34.2	339.8

Supplementary Table 5: Seabird-colony ammonia (NH_3) emissions. NH_3 emissions implemented in addition to the Riddick et al.[3,4] seabird-colony NH_3 inventory at latitudes between 70 °N and 90 °N.

Latitude (°N)	Longitude (°E)	Emissions (Mg NH_3 yr^{-1})
70.4	-148	9.2
71.4	53.4	766.8
73.1	-91.6	3.1
73.8	55.0	484.5
74.0	-90.0	124.3
74.5	19.0	190.0
74.8	-96.4	4.2
75.8	58.6	276.7
76.1	-68.7	96.6
76.6	-70.0	111.6
76.7	67.2	14.5
77.4	-72.0	286.9
80.4	57.7	43.6
80.6	49.2	3.4

Supplementary Methods:

Additional GEOS-Chem-TOMAS model description

Further details about the GEOS-Chem-TOMAS oxidant-aerosol tropospheric chemistry mechanism can be found in recent publications[5,6,7,8,9,10,11,12,13,14,15]. Further details about the TOMAS aerosol microphysics package are found in Lee and Adams[16]. The bin scheme that we used in our study was tested relative to higher-resolution bin schemes[16]. Lee and Adams[16] quantified that the error in prediction of the particle number larger than

70-100 nm was +/- 5% with varying resolution and the error associated with cloud processing and wet removal was within +/- 20%. Details about the approximation of particles smaller than 3 nm are provided in Kerminen et al.[17] and Lee et al.[18].

Additional Atmospheric Cluster Dynamics Code description

The Atmospheric Cluster Dynamics Code **(**ACDC) theoretical model as briefly described in Methods was used to calculate the ternary H_2SO_4–NH_3–H_2O particle formation rate by simulating the dynamics of a population of electrically neutral molecular clusters via numerical solution of the cluster birth–death equations. Here we provide additional details. Instead of considering only the collision and evaporation of single vapour molecules, an often-used perspective applied e.g. in the classical nucleation theory framework, ACDC allows all possible collision (molecule-molecule and molecule-cluster), coagulation (cluster-cluster), evaporation (molecule-cluster) and fission (cluster-cluster) processes within the population. For these simulations, the concentrations of gas-phase sulphuric acid and ammonia molecules are set to fixed values, and the birth–death equations are solved to obtain the steady-state formation rate at the given vapour concentrations. Sulphuric acid and ammonia molecules are considered explicitly in the simulations, while water molecules are taken into account implicitly by assuming equilibrium hydrate distributions for all sulphuric acid–ammonia clusters and molecules[19,20]. The rates of collision and coagulation were computed assuming each molecule and cluster behaved as hard spheres. The evaporation rates of constituents from the molecular clusters are a key parameter set with significant influence over the formation rates predicted by the model. In this case, they were derived from the Gibbs

free energies of formation of the clusters, which were calculated via quantum chemical methods at the B3LYP/CBSB7//RICC2/aug-cc-pV(T+d)Z level of theory[21,22]. Additionally, the scavenging of clusters by larger particles was accounted for by assuming an external sink term for all clusters.

Calculation of aerosol direct radiative effect

To calculate the all-sky aerosol direct radiative effect (DRE), we use monthly averaged aerosol mass and number concentrations from our GEOS-Chem-TOMAS simulations and refractive indices from the Global Aerosol Database[23]. We assume a core-shell morphology such that externally mixed black carbon forms a core surrounded by a homogenous shell composed of the other aerosol species. The refractive index of the homogeneously mixed shell is a volume-weighted average of the individual components. Optical depth, single scattering albedo, and the asymmetry parameter are calculated using coated-sphere Mie code (BHCOAT)[24]. The top-of-the-atmosphere flux is simulated using RRTMG. Monthly averaged surface albedo and cloud fraction are obtained from GEOS-5 meteorology. The summertime DRE due to the addition of seabird-colony NH_3 emissions was -0.03 W m^{-2} or less at all Arctic locations, and the pan-Arctic-mean DRE was -0.005 W m^{-2}.

Trace-gas and particle measurements

Here we provide additional references related to the AIM-IC instrument[25,26].

Supplementary References

1. Wexler, A. S. & Clegg, S. L. Atmospheric aerosol models for systems including the ions H^+, $NH4^+$, Na^+, $SO4^{2-}$, $NO3^-$, Cl^-, Br^- and H2O. *J. Geophys. Res.* **107**, D14, 4207 (2002).
2. Clegg, S. L. Brimblecombe, P. & Wexler A. S. Thermodynamic model of the system H^+ - $NH4^+$ - $SO4^{2-}$ - $NO3^-$ - H2O at tropospheric temperatures. *J. Phys. Chem. A* **102**, 2137-2154 (1998).
3. Riddick, S. N. *et al.* The global distribution of ammonia emissions from seabird colonies. *Atmos. Environ.* **55,** 319–327 (2012).
4. Riddick, S N. *et al.* Global ammonia emissions from seabirds. NERC Environmental Information Data Centre. doi:10.5285/c9e802b3-43c8-4b36-a3a3-8861d9da8ea9 (2012).
5. Park, R. J., Jacob, D. J., Field, B. D. & Yantosca, R. M. Natural and trans-boundary pollution influences on sulphate-nitrate-ammonium aerosols in the United States: Implications for policy, *J. Geophys. Res.* **109,** D15204 (2004).
6. Park, R. J., Jacob, D. J., Naresh, K. & Yantosca, R. M. Regional visibility statistics in the United States: Natural and trans-boundary pollution influences, and implications for the Regional Haze Rule, *Atmos. Environ.* **40,** 5405–5423 (2006).
7. Park, R. J., Jacob, D. J., Chin, M. & Martin, R. V. Sources of carbonaceous aerosols over the United States and implications for natural visibility, *J. Geophys. Res.* **108,** D15204 (2003).

8. Liao, H., Henze, D. K., Seinfeld, J. H., Wu, S. & Mickley, L. J. Biogenic secondary organic aerosol over the United States: Comparison of climatological simulations with observations, *J. Geophys. Res*. **112,** D06201 (2007).

9. Fairlie, T. D., Jacob, D. J. & Park, R. J. The impact of transpacific transport of mineral dust in the United States, *Atmos. Environ.* **41,** 1251–1266 (2007).

10. Fairlie, T.D. *et al.* Impact of mineral dust on nitrate, sulfate, and ozone in transpacific Asian pollution plumes. *Atmos. Chem. and Phys.* **10,** 3999-4012 (2010).

11. Alexander, B. *et al.* Sulfate formation in sea-salt aerosols: Constraints from oxygen isotopes. *J. Geophys. Res.* **110,** D10307 (2005).

12. Jaeglé, L., Quinn, P. K., Bates, T. S., Alexander, B. & Lin, J. T. Global distribution of sea salt aerosols: New constraints from in situ and remote sensing observations, *Atmos. Chem. Phys*. **11,** 3137–3157 (2011).

13. van Donkelaar, A. *et al.* Analysis of aircraft and satellite measurements from the intercontinental chemical transport experiment (INTEX-B) to quantify long-range transport of East Asian Sulfur to Canada. *Atmos. Chem. Phys.* **8**, 2999-3014 (2008).

14. Nightingale, P. D. *et al.* In situ evaluation of air-sea gas exchange parameterizations using novel conservative and volatile tracers. *Global Biogeochem. Cycles* **14,** 373-387 (2000).

15. Alexander, B., Park, R.J., Jacob, D. J. & Gong, S. Transition metal-catalyzed oxidation of atmospheric sulfur: global implications for the sulfur budget. *J. Geophys. Res.* **114,** D02309 (2009).

16. Lee, Y. H. & Adams, P. J. A Fast and Efficient Version of the TwO-Moment Aerosol Sectional (TOMAS) Global Aerosol Microphysics Model, *Aerosol Sci. Technol.* **46,** 678–689 (2012).

17. Kerminen, V. M., Anttila, T., Lehtinen, K. E. J. & Kulmala, M. Parameterization for atmospheric new-particle formation: Application to a system involving sulfuric acid and condensable water-soluble organic vapours, *Aerosol Sci. Technol*. **38,** 1001–1008 (2004).

18. Lee, Y.H., Pierce, J.R. & Adams, P.J. Representation of nucleation mode microphysics in global aerosol microphysics models, *Geosci. Model Dev*. **6,** 1221-1232 (2013).

19. Henschel, H., Kurtén, T. & Vehkamäki, H. Computational study on the effect of hydration on new particle formation in the sulfuric acid/ammonia and sulfuric acid/dimethylamine systems, *J. Phys. Chem. A.* **210,** 1886-1896 (2016).

20. McGrath, M. J. *et al.* Atmospheric Cluster Dynamics Code: a flexible method for solution of the birth-death equations. *Atmos. Chem. Phys.* **12,** 2345-2355 (2012).

21. Ortega *et al.* From quantum chemical formation free energies to evaporation rates. *Atmos. Phys. Chem.* **12,** 225-235 (2012).

22. Henschel, H. *et al.* Hydration of atmospherically relevant molecular clusters: Computational chemistry and classical thermodynamics. *J. Phys. Chem. A* **118,** 2599–2611 (2014).

23. Kopke, P., Hess, M., Schult, I. & Shettle, E. P. Global Aerosol Data Set, Report No. 243 Max Planck Inst. für Meteorol. Hamburg, Germany, ISSN 0937-1060 (1997).

24. Bohren, C. F. & Huffman, D. R. Absorption and scattering of light by small particles. Wiley Online Library. doi:10.1002/9783527618156 (2007).

25. VandenBoer, T. C., Petroff, A., Markovic, M. Z. & Murphy, J. G. Size distribution of alkyl amines in continental particulate matter and their online detection in the gas and particle phase, *Atmos. Chem. Phys.,* **11,** 4319-4332 (2011).

26. Markovic, M. Z., VandenBoer, T. C. & Murphy, J. G. Characterization and optimization of an online system for the simultaneous measurement of atmospheric water-soluble constituents in the gas and particle phases, *J. Environ. Mon.* **14,** 1872-1884 (2012).